# Evaluating Soil Surface Scattering Models: Perspectives From Polarimetric P-, L-, and S-Band SAR Observations

Ziwei Xiong, Jeffrey P. Walker, *Fellow, IEEE*, Liujun Zhu, *Member, IEEE*, Brian Ng, *Member, IEEE*, Nan Ye, Xiaoling Wu, *Senior Member, IEEE*, Lixiaozhou Zhou, *Member, IEEE*, Luisa F. White-Murillo, *Member, IEEE*, James Hills, Mahta Moghaddam, *Fellow, IEEE*, and Simon Yueh, *Fellow, IEEE*

***Abstract*—Recent advancements in spaceborne synthetic aperture radar (SAR) missions enable multifrequency soil moisture retrieval; however, the performance of standard surface scattering models at S- and P-bands remains largely underexplored compared to L-, C-, and X-bands. Accordingly, this study has evaluated three widely used surface scattering models (Dubois, Oh, and AIEM) across C-, S-, L-, and two alternative P-band frequencies using a combination of satellite and airborne data. These surface scattering models were also calibrated under two scenarios, one characterized by limited spatial and temporal variability and the other having considerable spatial and temporal variability. Results showed that the semi-empirical Dubois and Oh models performed reliably at L-band, with RMSE values around 2.4 dB. However, the AIEM model revealed large biases, underestimating or overestimating the backscatter by up to 6.5 dB. However, when calibrating these models against a dataset with similar temporal and spatial characteristics, the bias was reduced considerably, yielding an RMSE below 2 dB in most cases. Nonetheless, model performance deteriorated when applied to data with larger spatial and temporal characteristics, with RMSE increasing to ~3 dB. While the Dubois model outperformed the Oh model in terms of empirical adaptability, both models had poor performance at P-band, likely due to the dominance of subsurface scattering. Meanwhile, the AIEM model results were improved substantially at C-, S-, and L-band when calibrated, but its formulation based solely on surface scattering made it unsuitable for application to P-band, where subsurface contributions were considered to be substantial, especially when the surface was dry, and so could not be compensated through conventional roughness parameter adjustments. Overall, while calibration could enhance the performance of these semi-empirical and theoretical models under consistent temporal and spatial conditions, the greater penetration depth at P-band demands a more advanced scattering representation for accurate backscatter simulation.**

***Index Terms*—L-band, P-band, radar scattering model , S-band, soil moisture, synthetic aperture radar (SAR).**

## I. Introduction

NEAR-SURFACE soil moisture content is a key factor affecting hydrological, ecological, and biogeophysical activities [1]. Accurate soil moisture information is also vital for climate modeling, flood prediction, rainfall forecasting, evaporation rate determination, and precision agriculture [2]. Microwave remote sensing is widely acknowledged as the most reliable approach for mapping the near-surface soil moisture content, due to its direct relationship with the dielectric properties of wet soil [2], [3], [4], [5].

Among the microwave techniques, synthetic aperture radar (SAR) is considered the most effective for producing high spatial resolution soil moisture information [6], [7], making it particularly valuable for hydrological and agricultural applications [8], [9]. Accordingly, substantial efforts have been made to leverage spaceborne SAR observations for high-resolution soil moisture mapping, with most studies focused on L- and C-band due to their relatively longer wavelength and the availability of spaceborne data [10], [11]. More recently, satellite missions equipped with S- and P-band SAR instruments such as BIOMASS [12], NISAR [13], and NovaSAR-1 [14] are introducing new opportunities for soil moisture mapping. Notably, P-band SAR systems offer distinct advantages due to their enhanced penetration capabilities through vegetation canopies over rugged soil surfaces compared with L-band [15].

Retrieving near-surface soil moisture from SAR measurements generally involves the inversion of a scattering model that characterizes how soil moisture and surface roughness influence the backscattered radar signal. These include the Dubois et al. [16], [17], Oh et al. [18], [19], [20], and

Received 1 August 2025; revised 23 December 2025 and 20 January 2026; accepted 30 January 2026. Date of publication 10 February 2026; date of current version 24 February 2026. This work was supported in part by the National Natural Science Foundation of China under Grant 42371369; in part by Australian Research Council through the Research Discovery Grant DP170102373 and Grant DP210100430; and in part by the Linkage Infrastructure, Equipment, and Facilities under Grant LE0882509 and Grant LE190100045. *(Corresponding author: Liujun Zhu.)*

Ziwei Xiong and Liujun Zhu are with the State Key Laboratory of Water Disaster Prevention, Yangtze Institute for Conservation and Development, Hohai University, Nanjing 210024, China, and also with the Department of Civil and Environmental Engineering, Monash University, Clayton, VIC 3800, Australia (e-mail: ziwei.xiong@monash.edu; liujun.zhu@hhu.edu.cn).

Jeffrey P. Walker, Nan Ye, Xiaoling Wu, Lixiaozhou Zhou, and Luisa F. White-Murillo are with the Department of Civil and Environmental Engineering, Monash University, Clayton, VIC 3800, Australia.

Brian Ng is with The University of Adelaide, Adelaide, SA 5005, Australia.

James Hills is with the University of Tasmania, Hobart, TAS 7005, Australia.

Mahta Moghaddam is with the University of Southern California, Los Angeles, CA 90089 USA.

Simon Yueh is with the Jet Propulsion Laboratory, California Institute of Technology, Pasadena, CA 91109 USA.

Digital Object Identifier 10.1109/TGRS.2026.3663356

[21], integral equation model (IEM) [22], and its advanced version Advanced IEM (AIEM) [23]. The Dubois and Oh models are semi-empirical, meaning that they incorporate some physical understanding of scattering mechanisms while relying on empirical parameters derived from field or laboratory calibration. Although this approach makes them relatively straightforward to implement, their validity is generally restricted to conditions resembling those under which they were initially calibrated, specifically, the radar parameters (e.g., frequency, polarization, and incidence angle) and surface conditions (e.g., soil moisture and surface roughness). Consequently, application of these scattering models to different instruments or study sites often requires a recalibration [24], [25], [26].

In contrast to these semi-empirical models, the IEM and AIEM are theoretical (physical) models grounded in electromagnetic scattering theory, allowing broader applicability to diverse radar parameters without extensive site-specific calibration. However, they have not yielded consistently accurate results for all conditions, largely due to inaccuracies in characterizing the surface roughness relevant to each frequency band, which can introduce substantial errors into the simulated backscatter ($\sigma^0$) [24], [27], [28]. Specifically, the land surface roughness could have multiple length scales, which can be modeled by the fractal surface with a power law spectrum [29], with its scattering characteristics nominally accounted for by two-scale scattering models [30], [31]. Consequently, many studies have aimed to identify effective roughness parameters to replace direct measurements, thereby improving the ability of IEM or AIEM to replicate the observed $\sigma^0$ [32], [33], [34], [35], [36].

Despite extensive calibration and validation of surface scattering models at C- and L-band frequencies [25], [26], [33], [35], [37], [38], [39], [40], and efforts to retrieve the soil moisture profiles at P-band using multilayered scattering models [15], [41], [42], the evaluation of surface scattering models has been limited at S- and P-bands. Such an evaluation is important when considering that the P-band can penetrate deeper into the soil, meaning that its scattering cannot always be treated as solely a surface phenomenon. Consequently, it is unclear whether existing surface scattering models can be used reliably for near-surface soil moisture retrieval at P-band.

A related and unresolved question is whether model calibration can compensate for this limitation, given that the P-band lies outside the original design range of commonly used surface scattering models. Similar extensions beyond the nominal validity range have been explored at X-band, where physically meaningful backscatter simulations were achieved using calibrated IEM-, Oh-, and Dubois-based approaches over bare soils [52]. This precedent suggests that, under suitable conditions, calibration may at least partially extend model applicability beyond its intended frequency range. However, whether such calibration strategies remain effective at P-band has not yet been systematically assessed.

To address this gap, a comparative assessment of surface scattering models across multiple frequencies was made in this study, drawing on spaceborne C-band (5.045 GHz) and S-band (3.2 GHz) SAR data, as well as airborne L-band (1.26 GHz) and P-band (860 and 440 MHz) SAR data.

## II. Data

Data from two field campaigns were used in this study, being the P-band Radiometer Inferred Soil Moisture campaign undertaken in 2021 (PRISM21) and the first Active-Passive P- and L-band Experiment (APPLEx-1). Both campaigns were conducted in semi-arid grazing and agricultural regions near Yanco, Murrumbidgee Catchment, Australia (Fig. 1) using an experimental aircraft equipped with L- and P-band SARs to emulate spaceborne observations. PRISM21 was conducted from March 9 to 25, 2021, capturing six days of airborne observations that predominantly focused on passive measurements, yet also included active data. APPLEx-1 was conducted from January 27 to February 26, 2022, collecting nine days of both active and passive measurements. In addition to these airborne datasets, spaceborne Sentinel-1 C-band [43] and NovaSAR-1 S-band [14] data acquired during the same periods were also used, allowing for a comprehensive analysis of surface scattering models to be made across multiple frequency bands.

### A. Ground Soil Moisture

On flight days, intensive soil moisture measurements of near-surface (0–5 cm) soil moisture were conducted for 11 focus paddocks (Fig. 1). A portable soil moisture sensor called the hydraprobe data acquisition system (HDAS) [44] was employed to measure the near-surface soil moisture across each focus area or paddock with a spacing of 250 m for APPLEx-1 and 50 m for PRISM21. Depending on the ground surface complexity, 3–9 point-based soil moisture measurements were taken within a 1 m radius at each sampling location and averaged to represent the soil moisture content, thereby accounting for small-scale spatial variability. As illustrated in Fig. 1, soil moisture was measured and averaged at the paddock level within each campaign area. These paddock averages were subsequently used for model calibration and validation.

Surface soil roughness was characterized at each focus area using a pin or laser profiler. Each measurement consisted of two 3-m-long surface profiles taken in orthogonal directions. For nontilled areas, one profile was taken parallel to the flight line and the other perpendicular, while profiles were taken across and along the row direction for furrowed areas. To further characterize the paddocks and quantify vegetation structure, detailed vegetation sampling was conducted across all focus areas throughout the campaign, including the vegetation water content (VWC) kg/m$^2$.

### B. Airborne and Spaceborne Remote Sensing Data

A small experimental aircraft was used to perform the airborne SAR measurements. The remote sensing instruments included two SAR sensors: the Polarimetric L-band Imaging SAR (PLIS) and the Polarimetric P-band Imaging SAR (PPIS). PLIS operates at 1.26 GHz with a 30-MHz bandwidth and provides HH, HV, VH, and VV polarizations at a ground

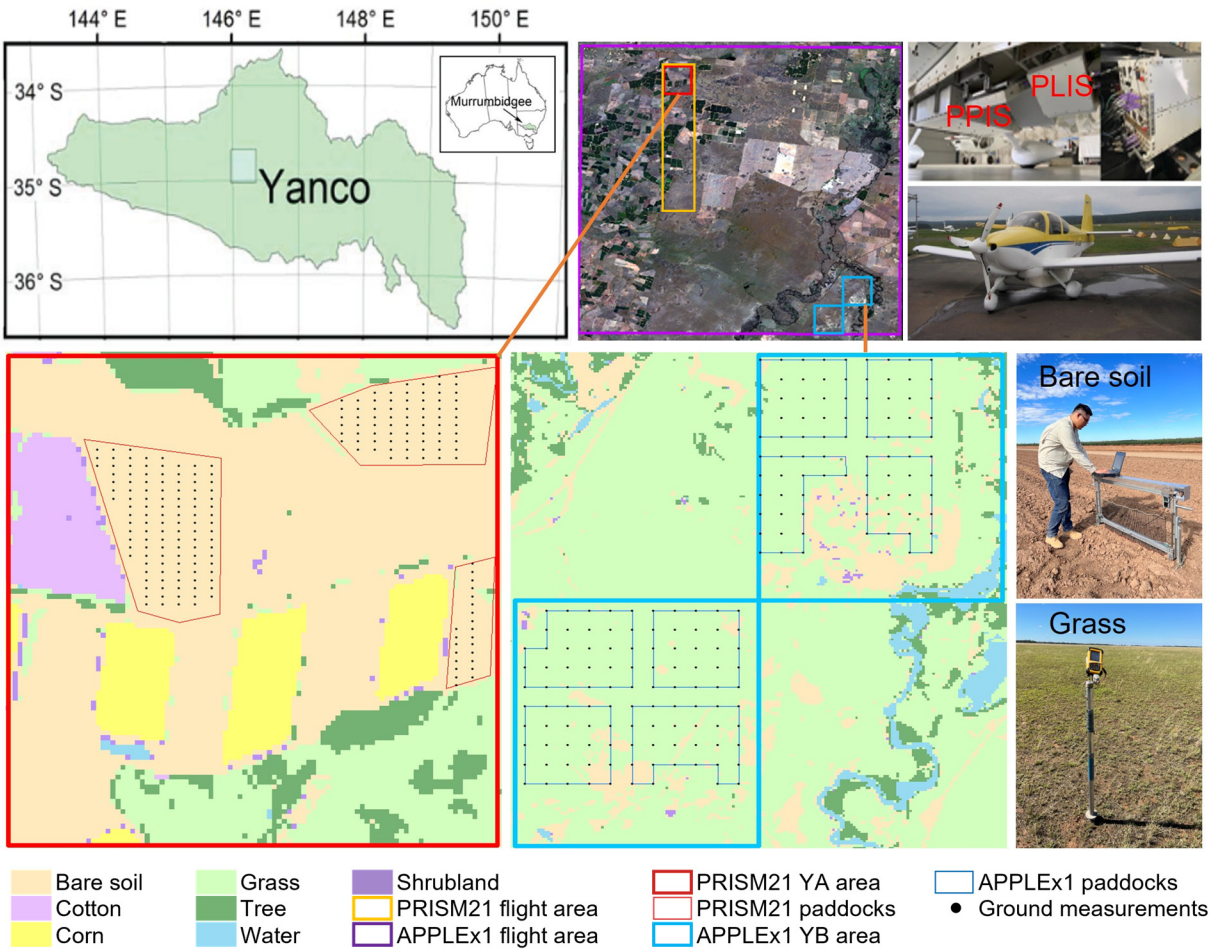


Fig. 1. Study area and datasets used from the APPLEx-1 and PRISM21 field campaigns. The figure shows the landcover map, paddock boundaries, flight areas, and ground-measurement locations, along with photographs of the airborne SAR instruments (PLIS and PPIS) and representative bare-soil and grass conditions.

resolution of about 10 m. PPIS operates at 860 MHz (20-MHz bandwidth) and 440 MHz (20-MHz bandwidth), delivering the same four polarizations at a ground resolution of about 15 m. The radar sensors were calibrated using forest-based observations and the responses from polarimetric active radar calibrators (PARCs) and passive radar calibrators (PRCs), following the detailed calibration steps provided in [38]. The residual radiometric error was found to be better than 1 dB over trihedral PRCs for PLIS and PPIS 440 MHz, and better than 1.5 dB for PPIS at 860 MHz.

During the APPLEx-1 campaign, airborne SAR data were acquired by cycling through three distinct flight configurations over the designated focus area every three days throughout a four-week experimental period. The SAR data from nine flight days were used, being those collected on January 31 and February 3, 6, 9, 11, 14, 17, 20, and 23, 2022. Similarly, SAR data for PRISM21 were collected on March 9, 13, 16, 18, 20, and 25, 2021. A key distinction between the two campaigns lies in their spatial coverage strategy. APPLEx-1 flights were designed with minimal spatial overlap to ensure full coverage of a $40 \times 40$ km area, while PRISM21 flights were overlapped with the intention to collect multi-incidence angle data over a 3-km swath of 20 km in length (Fig. 1).

Two NovaSAR-1 S-band acquisitions (January 31 and February 17, 2022) and two Sentinel-1 C-band acquisitions (February 9 and 21, 2022) were acquired during the APPLEx-1 campaign. While NovaSAR-1 did not acquire data during the PRISM21 period. Consequently, the limited number of available acquisitions from the satellite sensors constrained the extent of their application in this study.

Since there were only three pure bare soil paddocks observed with ground measurements during the two campaigns, eight low-vegetated grassland paddocks (where VWC was less than 0.3 kg/m$^2$) have also been treated as bare soil in order to provide a more comprehensive study. The effect of such sparsely vegetated areas on $\sigma^0$ has previously been found to be negligible for low frequencies [16], [45]. The ground data and focus paddocks for each campaign are summarized in Table I.

Backscatter simulations were conducted using the paddock-averaged incidence angle $\theta$, obtained from all SAR measurements within each paddock. While spaceborne $\theta$ remains

TABLE I
PROPERTIES OF THE PADDOCKS AND ASSOCIATED DATA USED IN THIS STUDY

| Paddock location | APPLEx-1 YB | PRISM21 YA |
|---|---|---|
| Landcover | Sparse Grass | Bare |
| Surface roughness [cm] | ~2 | ~1.6 |
| Soil moisture range [$m^3/m^3$] | 0.002-0.457 | 0.020-0.400 |
| # ground measurement [per day] | ~125 | ~140 |
| # days airborne data | 9 | 6 |
| # days satellite data | 2 | N.A. |

nearly constant across paddocks, airborne $\theta$ varies across flight lines, and thus paddocks, due to the side-looking antenna geometry from a much lower altitude. Motion-compensation procedures were applied to reduce variability due to small aircraft pitch/roll/yaw movements. Importantly, the within-paddock variation of incidence was typically 3°–5°, which is minimal. Therefore, using the paddock-averaged $\theta$ provided a representative incidence angle for each focus area while avoiding the modeling errors that would arise if a single site-wide angle were assumed.

## III. METHOD

### A. Scattering Models

The commonly used Dubois, Oh, and AIEM models were used in this study, with their validity conditions and calibration methods given in Table II. The Dubois model is a semi-empirical approach developed to estimate $\sigma^0$ over bare soil surfaces using scatterometer data across frequencies ranging from 1.5 to 11 GHz [16], [17]. Similarly, the Oh model was proposed based on theoretical models, scatterometer measurements, and airborne SAR observations of bare soils. Its original expressions for co-polarization and cross-polarization ratios ($p$ and $q$) were empirically derived using ground-based measurements [18]. Subsequent studies introduced refinements to account for incidence angle effects [19], proposed revised formulations for $p$ and $q$ along with a method to calculate cross-polarized $\sigma^0$ [20], and ultimately proposed a simplified formula for $q$ that excludes the correlation length due to its minimal sensitivity and the difficulty of measuring it accurately in the field [21], [28], [46]. The latest version of the Oh [21] model was used in this study. Wu and Chen [23] extended the original IEM [22] to the AIEM, which replaces the Fresnel reflection coefficients with a transition function that accounts for both surface roughness and soil permittivity. This modification was designed to reduce the uncertainties and sensitivity issues typically associated with roughness parameter estimation in the original model. The improvements have been demonstrated by both numerical simulations and real measurements.

In these models, the soil is treated as a pure surface scatterer or emitter, with the topmost soil layer assumed as a homogeneous dielectric medium. This simplification is based on the understanding that contributions of subsurface scattering from the root zone in the soil strata relative to the total $\sigma^0$ are generally small and decrease rapidly with increasing soil moisture content [47]. Consequently, these bare soil models neglect subsurface scattering and estimate $\sigma^0$ based solely on the geometric and dielectric properties of the soil surface. Moreover, the geometric properties of the soil surface are commonly described using the roughness root-mean-square height and autocorrelation length [48], while the dielectric properties controlled by soil moisture and textural composition [49]. These models generally predict a monotonic increase in $\sigma^0$ with increasing near-surface soil moisture, independent of roughness conditions. Therefore, the retrieved soil moisture is typically interpreted as being an effective value representing the average soil moisture content within the top 5-cm soil layer. Many studies have demonstrated that such concepts are suitable for multiple frequencies, including X-, C-, and L-bands [25], [37], [50].

Although the semi-empirical surface scattering models were originally proposed for frequencies at or above L-band, they have also been applied to data outside their original calibration range [25]. The validity range primarily reflects the domain of the data used during model development and should therefore be interpreted as an indicator of optimal performance rather than as a strict threshold for applicability. Naturally, the models are expected to be applicable to S-band data, as it lies between L- and C-band in terms of frequency. However, there is a lack of studies validating its effectiveness at this frequency. While this assumption of surface-only scattering may be less valid for P-band due to its greater penetration depth and the potential for more substantial subsurface scattering than in the current well-studied frequencies, these models are expected to still be useful for near-surface soil moisture retrieval when the contribution from deeper layers remains limited. Nevertheless, it remains valuable to evaluate whether these models, after appropriate calibration, can still accurately predict $\sigma^0$ at the P-band. Accordingly, this study has assessed the feasibility of extending surface scattering models to S- and P-band frequencies by analyzing the correlation between observed and modeled $\sigma^0$, particularly under conditions where conventional surface scattering assumptions may be challenged by increased subsurface contributions.

### B. Calibration Methods of Scattering Models

Since the aforementioned models were originally designed for frequencies higher than P-band, this study not only applied them directly to P-band data but also introduced calibration-based modifications to extend their applicability to P-band and improve their performance across other frequency ranges. These modifications and adjustments are summarized in Table II.

Extensive research has already evaluated the performance of the semi-empirical Dubois and Oh models at X-, C-, and L-bands, with some making an empirical calibration of the roughness parameter [24], [25], [26]. While these approaches

TABLE II

VALIDITY CONDITION, EXPRESSION OF SURFACE SCATTERING MODELS, AND THEIR CALIBRATION METHOD, WHERE $M_V$ IS THE SOIL MOISTURE CONTENT, $\varepsilon_r$ IS THE REAL PART OF THE SOIL DIELECTRIC CONSTANT, $k$ IS THE WAVENUMBER IN AIR, $s$ IS THE ROOT-MEAN-SQUARE HEIGHT OF THE SOIL SURFACE, AND $(\theta_i, \varphi_i)$ AND $(\theta_s, \varphi_s)$ ARE THE ELEVATION AND AZIMUTH ANGLES FOR THE INCIDENT AND SCATTERED RADIATION, RESPECTIVELY. $I^n_{pq}$ IS A FUNCTION COMPOSED OF KIRCHHOFF AND COMPLEMENTARY FIELD COEFFICIENTS AS DEFINED IN [23] AND [51], AND $W^{(n)}$ IS THE FOURIER TRANSFORM OF THE $n$TH POWER OF THE NORMALIZED SURFACE CORRELATION FUNCTION. IN THIS TABLE $\sigma^s$ DENOTES THE BISTATIC SCATTERING COEFFICIENT, WHEREAS $\sigma^0$ IS RESERVED FOR THE BACKSCATTERING COEFFICIENT WHEN $\theta_i = \theta_s$

| Model | Validity condition | Model expression | Calibration methods |
|---|---|---|---|
| Dubois | $ks \le 2.5$, $M_v \le 0.35$, and $\theta \ge 30°$ | $\sigma^0_{\mathrm{HH}} = 10^{-a}\left(\frac{\cos^b\theta}{\sin^s\theta}\right)10^{c\varepsilon_r\tan\theta}\lambda^{0.7}(k\,s\,\sin\theta)^{1.4}$, $\sigma^0_{\mathrm{VV}} = 10^{-d}\left(\frac{\cos^e\theta}{\sin^3\theta}\right)10^{f\varepsilon_r\tan\theta}\lambda^{0.7}(k\,s\,\sin\theta)^{1.1}$ | Modify the parameters in expression: $a = 2.75, b = 1.5, c = 0.028$, $d = 2.35, e = 3, f = 0.046$. |
| Oh | $0.13 \le ks \le 6.98$, $0.04 \le M_v \le 0.291$ and $10° \le \theta \le 70°$ | $\sigma^0_{\mathrm{VH}} = \boldsymbol{a}M_v^{\mathbf{b}}(\cos\theta)^{\boldsymbol{c}}\{1-\exp[-0.32(k\,s)^{1.8}]\}$, $q = \frac{\sigma^0_{\mathrm{VH}}}{\sigma^0_{\mathrm{VV}}} = 0.095(0.13+\sin1.5\theta)^{1.4}\{1-\exp[-1.3(k\,s)^{0.9}]\}$, $p = \frac{\sigma^0_{\mathrm{HH}}}{\sigma^0_{\mathrm{VV}}} = 1-(\frac{\theta}{90^o})^{dM_v^{-0.65}}\exp[-0.4(k\,s)^{1.4}]$. | Modify the parameters in expression: $a = 0.11, b = 0.7$, $c = 2.2, d = 0.35$. |
| AIEM | $ks \le 3$ | $\sigma^s_{\mathrm{soil},pq} = \frac{k^2}{2}\exp[-s^2(k_z^2+k_{sz}^2)] \cdot\sum_{n=1}^{\infty}\frac{s^{2n}}{n!}\left\|I^n_{pq}\right\|^2 W^{(n)}(k_{sx}-k_x, k_{sy}-k_y)$, $k_x = k\sin\theta_i\cos\varphi_i;\ k_{sx} = k\sin\theta_s\cos\varphi_s;$ $k_y = k\sin\theta_i\sin\varphi_i;\ k_{sy} = k\sin\theta_s\sin\varphi_s;$ $k_z = k\cos\theta_i;\ k_{sz} = k\cos\theta_s$ | Apply the $L_{opt}$: C-band: $L_{\mathrm{opt(C)}}(s,\theta,\mathrm{HH}) = 0.162 + 3.006(\sin1.23\theta)^{-1.494}s$, $L_{\mathrm{opt(C)}}(s,\theta,\mathrm{VV}) = 1.281 + 0.134(\sin0.19\theta)^{-1.59}s$, L-band: $L_{\mathrm{opt}(L)}(s,\theta,\mathrm{HH}) = 2.65\theta^{-1.4493} + 3.0484s\theta^{-0.8044}$, $L_{\mathrm{opt}(L)}(s,\theta,\mathrm{VV}) = 5.8735\theta^{-1.0814} + 1.3015s\theta^{-1.4498}$, S-band: $L_{\mathrm{opt(S)}}(s,\theta,\mathrm{HH}) = 0.5\times(L_{\mathrm{opt(C)}}(s,\theta,\mathrm{HH}) + L_{\mathrm{opt}(L)}(s,\theta,\mathrm{HH}))$, $L_{\mathrm{opt}(S)}(s,\theta,\mathrm{VV}) = 0.5\times(L_{\mathrm{opt(C)}}(s,\theta,\mathrm{VV}) + L_{\mathrm{opt}(L)}(s,\theta,\mathrm{VV}))$, P-band: $L_{\mathrm{opt}(P)}(s) = ks$. |

were effective within the originally validated frequency ranges of the respective models, their extension to P-band is expected to be more challenging due to the fundamentally different scattering mechanisms associated with deeper signal penetration. To address this challenge, sensitivity analysis was conducted to identify model parameters that exhibit strong sensitivity to both soil moisture and frequency. These parameters were subsequently used as calibration variables and optimized using representative training datasets.

For the AIEM model, it is widely acknowledged that accurate measurement of surface roughness parameters is challenging, particularly the correlation length, often leading to large discrepancies between simulated and measured $\sigma^0$ [32], [52]. Typically, an effective correlation length ($L_{\mathrm{opt}}$) is used as a semi-empirical calibration parameter for the AIEM, where the in situ measured correlation length is replaced with a fitting parameter $L_{\mathrm{opt}}$. This effective value depends on surface roughness conditions, being also influenced by the

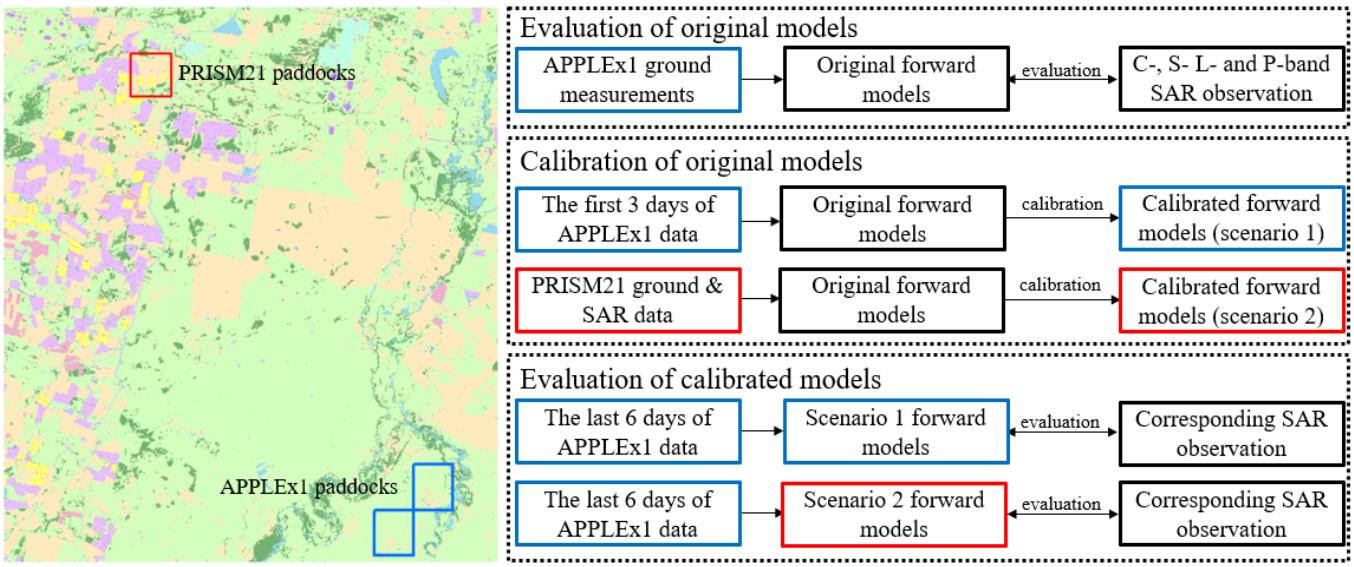


Fig. 2. Flowchart illustrating the SAR data arrangement and the validation process of surface scattering models across multiple frequencies, incorporating ground measurements, model calibration, and evaluation with corresponding SAR observations.

SAR configuration, such as incidence angle, polarization, and radar wavelength. Previous studies have calibrated $L_{\text{opt}}$ using extensive experimental datasets at C-band [53] and L-band [35]. These parameterizations were adopted in this study.

As no established $L_{\text{opt}}$ parameterizations currently exist for S- and P-bands, and the datasets used in this study were not sufficiently large to derive comparable empirical equations, the following strategies were implemented so as to enable similar calibration at these frequencies. Since the S-band lies between C- and L-bands, the average of the C- and L-band $L_{\text{opt}}$ equation was applied to the S-band data. For the P-band, a simplified approach was adopted by directly matching the modeled and observed $\sigma^0$. The optimized parameters were determined by minimizing the cost function

$$\text{Cost function} = \sqrt{\sum_{i=1}^{n} (\sigma^0_{i,\text{obs}} - \sigma^0_{i,\text{mod}})^2 + (1 - \text{slope})^2} \quad (1)$$

which considers both the difference between the observed and modeled $\sigma^0$ and slope for $n$ samples.

### C. Evaluation and Calibration Scenarios

The original surface scattering models were first evaluated using the APPLEx-1 dataset, with two calibration and validation scenarios designed to comprehensively evaluate the potential of the calibrated models (Fig. 2), especially the ability of the calibrated model for near-surface soil moisture retrieval.

In scenario 1 (S1), model calibration was performed using data from the first three acquisition dates of the APPLEx-1 campaign over the low-vegetated grassland site in the YA region. The remaining dates and sites were reserved for validation. This setup enabled the assessment of model performance under spatially consistent conditions and across a relatively short temporal interval.

In scenario 2 (S2), the models were calibrated using bare-soil data from the PRISM21 campaign and validated with low-vegetated grassland data from the APPLEx-1 YA site. This arrangement allowed for the evaluation of model robustness under conditions of extended temporal separation and differing spatial characteristics. Due to limited data availability, the S- and C-band frequencies were calibrated under scenario 1 only. For these frequencies, one acquisition date was used for calibration and the other for validation of both the Dubois and Oh models.

## IV. Results

### A. Evaluation of the Naive Scattering Models

The daily averaged $\sigma^0$ observations from PLIS, PPIS860, and PPIS440 over the nine days during APPLEx-1 were compared with simulations from the original Dubois, Oh, and AIEM models.

Fig. 3(a) and (b) shows the results for C- and S-bands, respectively. The observed $\sigma^0$ exhibited weak or nearly no correlation with the model outputs and little slope with soil moisture. This may be attributed to the very limited soil moisture range (0–0.15 $m^3$) and the small size of the dataset. Additionally, the lack of correlation in the C-band data may be further explained by its larger interactions with the grass canopy compared to the S-band. Notably, a large bias was observed between the C-band VV and the AIEM simulations, resulting in an RMSE of 21.5 dB. This aligns with previous studies [26], highlighting the high sensitivity of the AIEM model to roughness parameters. In contrast, relatively lower RMSE values of 4.4, 3.8, and 3.2 dB were observed for the Dubois model at C-band VV and for the Oh and AIEM models at S-band HH, respectively.

Fig. 3(c) and (d) shows that the modeled $\sigma^0$ at L-band had the highest level of correlation with SAR backscatter and the highest slope with soil moisture among all frequencies. This can be partly explained by the larger dataset at L-band, being collected across a relatively larger soil moisture range. Another

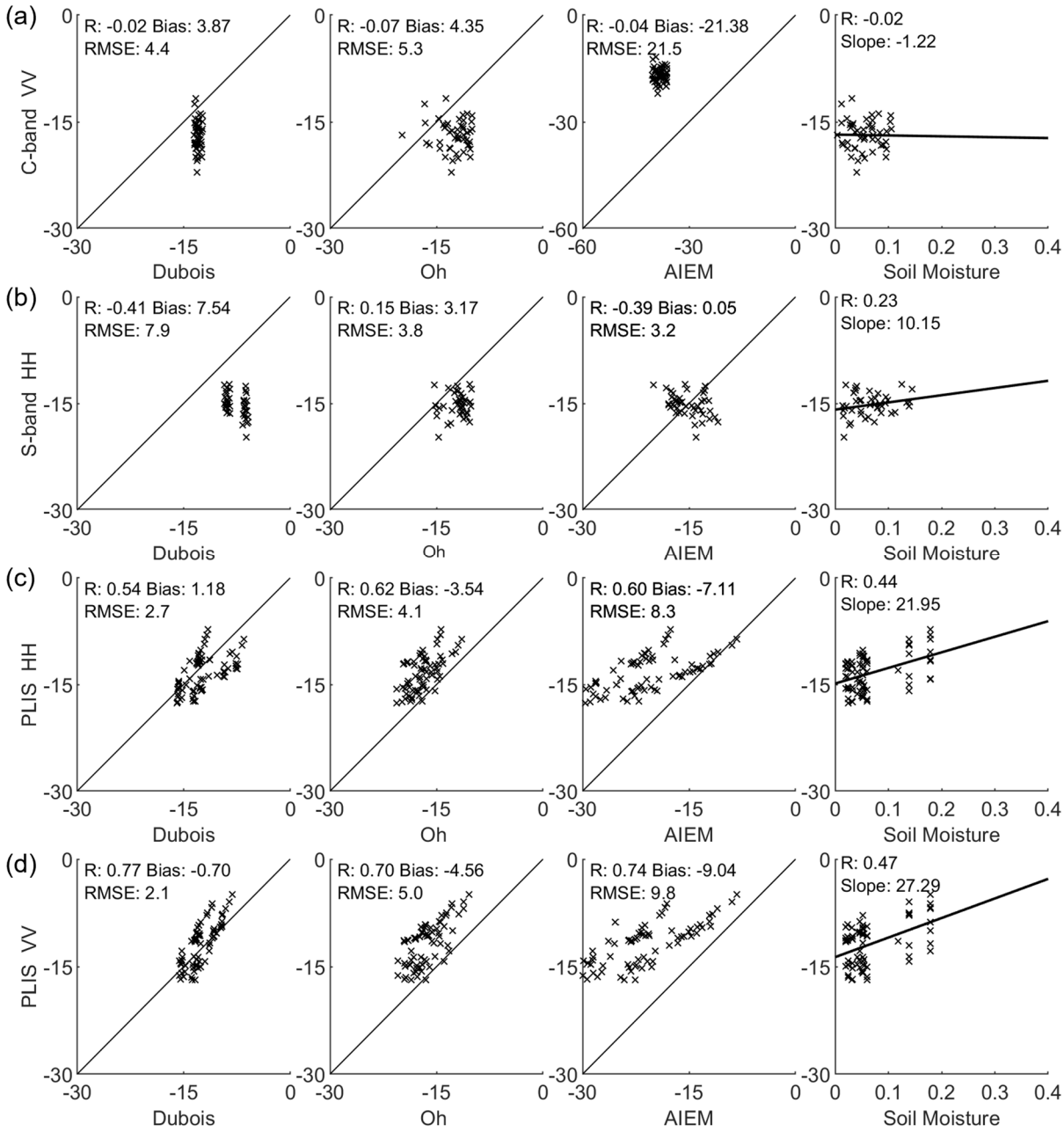


Fig. 3. Comparison between observed ($y$-axis) and simulated ($x$-axis) $\sigma^0$ (dB) from the original models over the YB area. Columns 1–3 show the scatterplots of SAR observations versus modeled $\sigma^0$ from Dubois, Oh, and AIEM models, respectively. Column 4 shows scatterplots of SAR observations versus near-surface soil moisture ($m^3/m^3$); the regression line and slope are provided for reference. Results are presented for (a) C-band VV polarization, (b) S-band HH polarization, (c) L-band HH polarization, and (d) L-band VV polarization. The C-band AIEM subplot uses an extended $x$-axis and $y$-axis scale to capture the full range of observations.

reason is that the L-band falls within the valid frequency range for these forward models. The two clusters visible in some panels arise from the presence of two distinct incidence angle groups (22°–27° and 34°–41°) across paddocks, leading to systematic offsets in the predicted–observed $\sigma^0$ relationship, a behavior that has also been reported in previous multifrequency SAR studies over bare soils [56]. The Dubois model achieved the best performance among the three, achieving an RMSE of 2.1 and 2.7 dB in VV and HH, respectively. In contrast, the Oh model showed substantial underestimation of $\sigma^0$ in both co-polarizations by 3–4 dB. The AIEM model performed the worst, underestimating the high values but overestimating the low values, with the overall bias ranging from −7 to −9 dB.

Fig. 4(a) and (b) presents the results for P-band HH and VV polarization at 860 MHz. Among all tested frequencies, SAR observations at this frequency achieved the highest correlation with near-surface soil moisture, being 0.44 for HH and 0.59 for

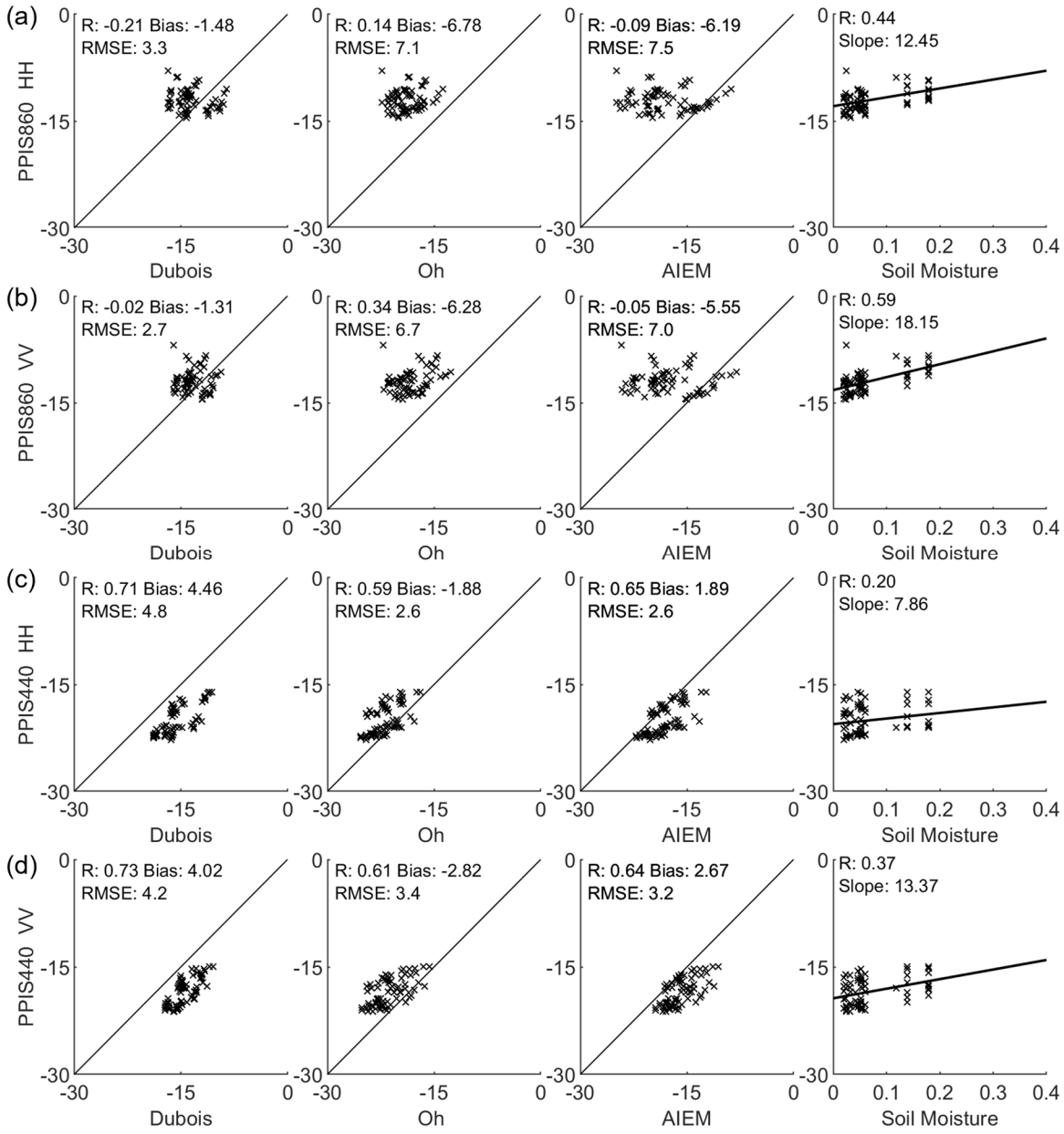


Fig. 4. Similar to Fig. 3, but for P-band observations and simulations from the original models. Results are shown for (a) P-band HH pol at 860 MHz, (b) P-band VV pol at 860 MHz, (c) P-band HH pol at 440 MHz, and (d) P-band VV pol at 440 MHz.

VV, while the slopes with soil moisture were less than that of L-band indicating weaker relationships and possible subsurface scattering contribution and possible contributions from subsurface scattering. However, the modeled $\sigma^0$ still showed a weak correlation with the observed values (<0.34), and in some instances, even negative correlations were observed. The Dubois model achieved a relatively low RMSE for both co-polarizations (3.3 dB for HH and 2.7 dB for VV), while the Oh and AIEM model tended to underestimate the $\sigma^0$, with a negative bias of around 6 dB. The higher instrument noise floor at 860 MHz may partly explain the weak agreement between the observed and modeled $\sigma^0$. The strong correlation between $\sigma^0$ and near-surface soil moisture and the inability of surface scattering models to reproduce this relationship suggest that direct use of these models to simulate $\sigma^0$ at 860 MHz could result in considerable errors and misinterpretation.

Fig. 4(c) and (d) presents the results for the P-band 440 MHz. Although this frequency lies well outside the intended validity range of the models, the modeled $\sigma^0$ for both HH and VV polarizations obtained a relatively high correlation with the corresponding SAR observations, ranging from 0.59 to 0.73, and were comparable to those observed at L-band. This may be attributed to the lower sensitivity of the P-band signal to surface roughness and thus the uncertainties in modeling roughness effects. However, the increased penetration depth of the P-band signal decreases its sensitivity

TABLE III
CALIBRATED OH AND DUBOIS MODEL PARAMETERS AND THEIR CORRESPONDING RESIDUAL RMSE FOR EACH SCENARIO. THE NAIVE PARAMETERS ARE THESE FROM THE ORIGINAL PUBLICATIONS

| **Model parameters** | **Naive** | **Scenario 1** | | | | | **Scenario 2** | | |
|---|---|---|---|---|---|---|---|---|---|
| **Oh** | [21] | PLIS | PPIS 860 | PPIS 440 | C | S | PLIS | PPIS 860 | PPIS 440 |
| $a$ | 0.110 | 0.500 | 0.078 | 0.085 | 0.002 | 0.005 | 1.031 | 0.318 | 0.329 |
| $b$ | 0.700 | 0.716 | 0.510 | 0.297 | -0.482 | 0.037 | 0.873 | 0.418 | 0.576 |
| $c$ | 2.200 | 4.779 | -3.625 | 3.540 | 3.437 | -2.912 | 5.889 | 4.397 | 2.013 |
| $d$ | 0.350 | 0.210 | 0.734 | 0.257 | / | 0.309 | 0.293 | 0.855 | 0.244 |
| **Residual RMSE (dB)** | / | 2.226 | 1.754 | 1.652 | 1.770 | 1.174 | 3.490 | 2.087 | 2.651 |
| **Dubois** | [17] | PLIS | PPIS 860 | PPIS 440 | C | S | PLIS | PPIS 860 | PPIS 440 |
| $a$ | 2.750 | 3.139 | 3.268 | 3.399 | / | 3.350 | 2.750 | 2.776 | 3.044 |
| $b$ | 1.500 | -0.895 | -0.171 | -1.461 | / | -1.238 | 1.500 | -0.947 | -1.596 |
| $c$ | 0.028 | 0.059 | 0.125 | 0.020 | / | -0.012 | 0.028 | 0.019 | 0.015 |
| $d$ | 2.350 | 1.975 | 2.675 | 3.007 | 2.430 | / | 2.274 | 2.022 | 2.383 |
| $e$ | 3.000 | 4.746 | -0.203 | 0.460 | -1.328 | / | 3.608 | 4.056 | 3.011 |
| $f$ | 0.046 | 0.038 | 0.087 | 0.051 | -0.134 | / | 0.069 | 0.020 | 0.040 |
| **Residual RMSE (dB)** | / | 2.376 | 1.669 | 1.740 | 1.724 | 1.170 | 3.300 | 1.933 | 2.868 |

to near-surface soil moisture, as indicated by the slope with soil moisture being further decreased compared to 860 MHz, and the low correlation values between SAR observations and near-surface soil moisture, which was 0.2 for HH and 0.37 for VV at 440 MHz. Consequently, the semi-empirical models struggled to accurately predict $\sigma^0$ at this frequency. The Dubois model, in particular, produced substantial errors, with underestimation and overestimation reaching up to 4.8 dB at HH polarization. In contrast, the AIEM model performed relatively well, with a bias of approximately 2 dB. This may result from the reduced influence of surface roughness, which helps to offset the primary limitation of the AIEM in accurately parameterizing roughness effects. However, as a purely physical surface scattering model, the AIEM does not account for subsurface scattering. This likely reduces its accuracy at P-band frequencies where subsurface contributions to $\sigma^0$ are more prominent.

### *B. Calibration Solutions for the Scattering Models*

Calibration of the Dubois, Oh, and AIEM models was made in two calibration scenarios (Fig. 2). The calibrated parameters and the corresponding residual RMSE for the training dataset are summarized in Table III. For the S- and C-band data, although relatively low residual RMSE values were achieved with both the Dubois and Oh models, the small dataset size, the limited soil moisture variability, and the narrow range of incidence angles at these frequencies made it difficult to derive robust and generalizable model parameters. This limitation is more apparent in the validation results in Section IV-C. In contrast, the optimized parameters obtained for L-band under both calibration scenarios were generally consistent with those of the original models. This similarity was particularly evident for the Dubois model at HH polarization under scenario 2, where the optimized parameters well matched those of the original model. In contrast, the calibrated parameters for P-band showed substantial deviations from the original values and differed considerably between scenarios 1 and 2. These differences suggest that the semi-empirical models may not effectively capture the scattering behavior at the P-band frequencies tested. Overall, the use of calibrated parameters resulted in lower residual RMSE values in the training datasets. However, scenario 2 produced higher residual RMSE values, possibly due to differences in surface roughness conditions among the PRISM21 bare soil paddocks.

The proposed calibration approach for the AIEM model was ineffective at the two P-band frequencies, as the model consistently underestimated the $\sigma^0$ and failed to produce valid solutions for the effective roughness parameter $L_{\text{opt(P)}}$. This underestimation became more pronounced as the frequency decreased from 860 to 440 MHz, suggesting that subsurface volume scattering plays an increasingly important role at lower frequencies and contributes a larger proportion of the total $\sigma^0$. Consequently, the AIEM model, which is based only on surface scattering physics, is not suitable for simulating $\sigma^0$ at P-band frequencies. The effect of subsurface scattering cannot be adequately compensated by applying the widely used effective roughness. Ideally, a scattering model that incorporates both surface and subsurface contributions would be more suitable for simulating P-band $\sigma^0$. However, this was beyond the scope of the current study.

### *C. Evaluation of Calibrated Scattering Models*

After obtaining the optimized model parameters under the two calibration scenarios, the modified scattering models were validated using an unseen dataset collected from the

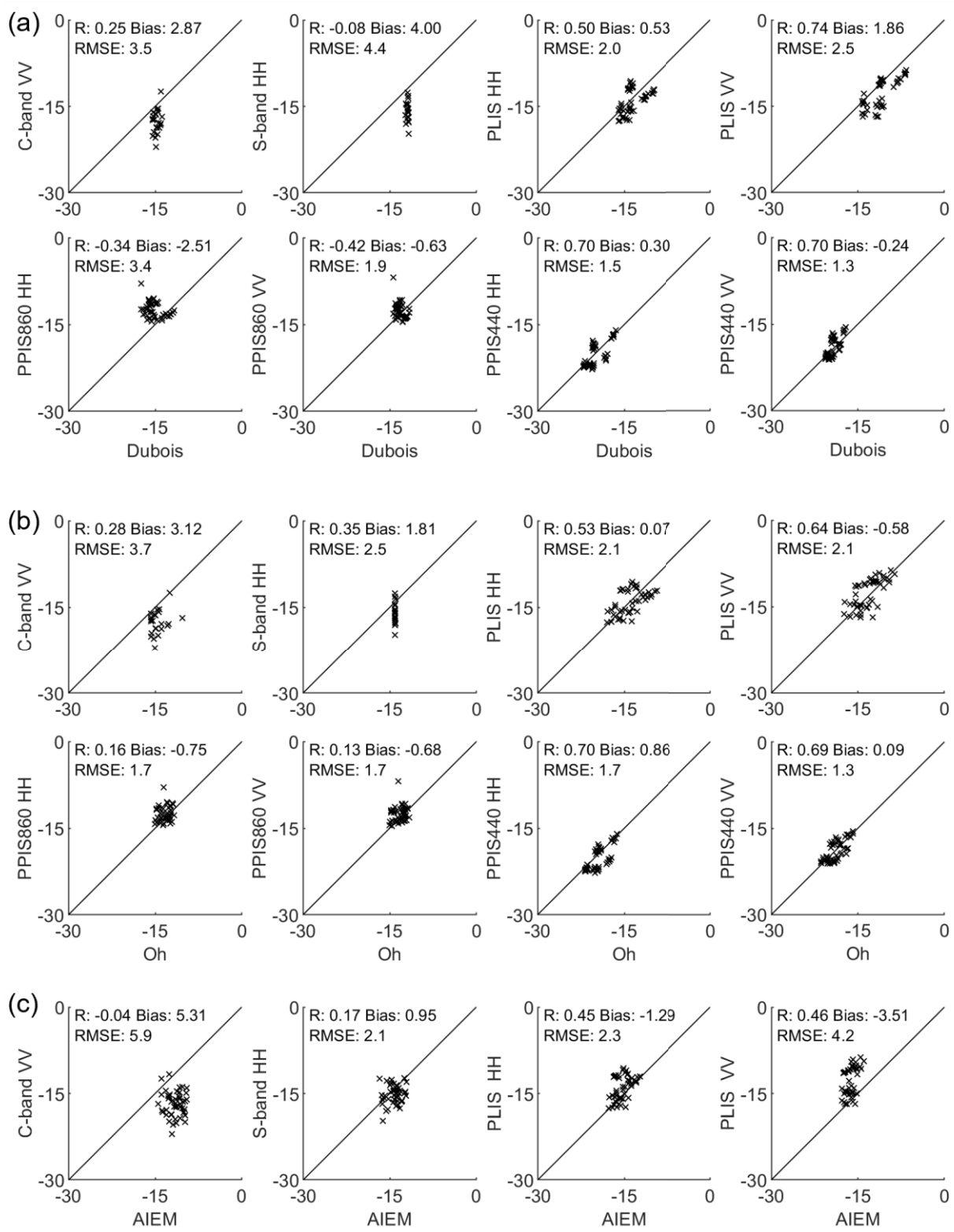


Fig. 5. Comparison between measured and simulated $\sigma^0$ (dB) from the calibrated models for scenario 1, evaluated with three modeling approaches. (a) Dubois, (b) Oh, and (c) AIEM. Within each subfigure, results are shown for C-band (VV), S-band (HH), L-band (PLIS VV, HH), and P-band (PPIS860 and PPIS440 VV, HH).

APPLEx-1 YA sparsely vegetated grassland area. As illustrated in Fig. 5(a), the calibration of the Dubois model reduced the RMSE by ~0.9 dB at both C-band and S-band, primarily due to a reduction in bias by ~1 dB. However, a residual bias exceeding 3 dB remained, indicating limited model robustness, likely a result of the small size of the training set.

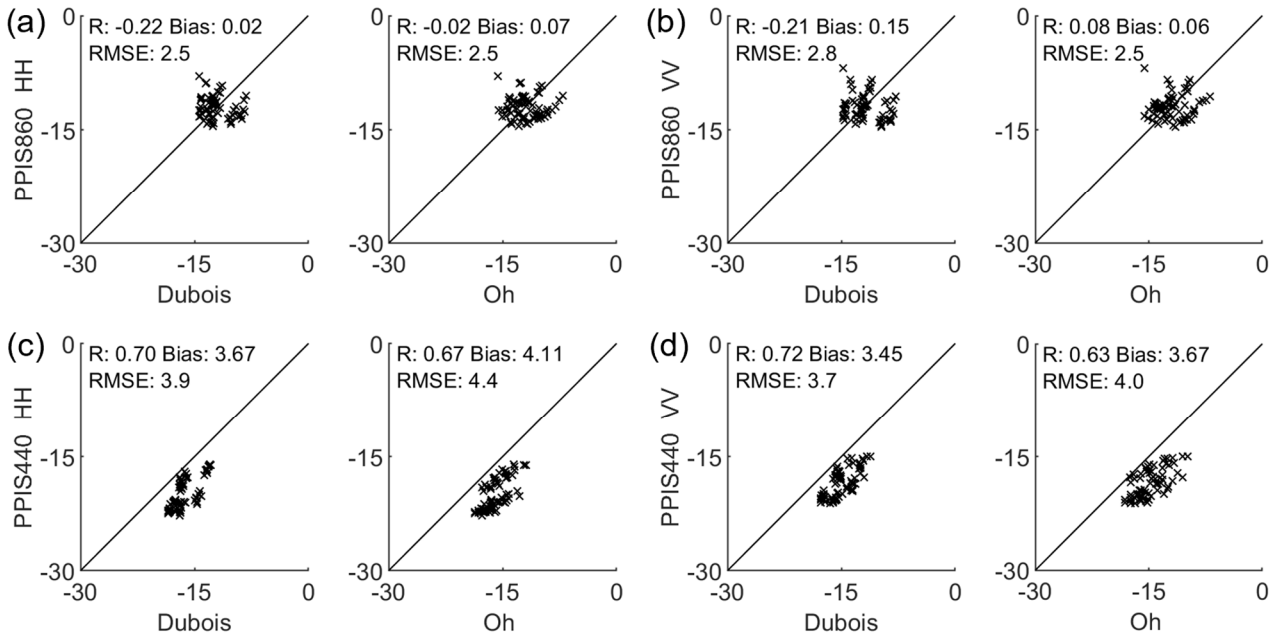


Fig. 6. Similar to Fig. 5, but models were calibrated under scenario 2. The semi-empirical model results are presented for P-band at 860 MHz (a) HH pol and (b) VV pol. P-band at 440 MHz (c) HH pol and (d) VV pol.

At P-band, only a moderate improvement was observed at P-band 860 MHz, while substantial improvement was achieved at 440 MHz, with a high R of ~0.7 for both co-polarizations and a low RMSE of 1.5 dB for HH and 1.3 dB for VV. In contrast, only a marginal improvement was made at L-band, where the calibrated model achieved an RMSE of 2.0 dB and an R value of 0.5 for HH polarization. These results were comparable to those of the original scattering model. For P-band frequencies, the calibrated scattering model had a considerably reduced RMSE, especially at 440 MHz, where RMSE fell below 2 dB. However, the R at 860 MHz remained below 0.2, having a similar performance to the uncalibrated scattering models.

Fig. 5(b) presents the validation results for the Oh model. Calibration led to reduced RMSE values at both C- and S-bands, with a notable improvement at S-band, where the RMSE decreased to approximately 2.1 dB. As expected, changes at L-band were minimal, consistent with the fact that the scattering model was originally developed for L-band. However, considerable improvements were observed at P-band, where the RMSE for both 860 and 440 MHz reduced to less than 1.7 dB. Despite these satisfactory reductions in RMSE, R at 860 MHz remained below 0.2.

Fig. 5(c) shows the results for the AIEM model. The semi-empirical calibration of $L_{\text{opt}}$ markedly reduced the RMSE at C-band to approximately 5.9 dB, largely due to a substantial correction of the model bias by about 16 dB. An even greater improvement was observed at S-band, where the RMSE dropped to ~2.1 dB. At L-band, the bias decreased from ~8 to 2 dB, highlighting the effectiveness of roughness parameter calibration in improving scattering model performance across multiple frequencies.

Fig. 6(a) and (b) presents the results for the calibrated 860-MHz scattering models under scenario 2. Overall, the scattering model performance deteriorated compared to scenario 1, where the RMSE decreased by approximately 0.6 dB for both Dubois and Oh models and R further decreased, approaching zero. Fig. 6(c) and (d) illustrates the results for the calibrated 440-MHz scattering models under scenario 2. Both scattering models showed a distinct trend toward overestimating $\sigma^0$. Scenario 2 produced considerably higher biases of around 4 dB, being much larger than those achieved in scenario 1 achieving ~1 dB. This led to an increased RMSE of approximately 2–3 dB.

Daily averaged $\sigma^0$ observations from PLIS and PPIS at 860 and 440 MHz were compared with the corresponding simulations derived from the original and calibrated Dubois, Oh, and AIEM models, where applicable. Since VV polarization exhibited similar temporal trends to HH polarization, only the HH results are presented. As illustrated in Fig. 7, PLIS consistently displayed higher R values compared to PPIS at 860 and 440 MHz, reflecting the greater sensitivity of shorter wavelengths to near-surface soil properties. The original scattering models generally captured the observed temporal trends at L-band, although the AIEM model demonstrated a notably larger bias than the Dubois and Oh models. At the lower P-band frequencies, $\sigma^0$ values were generally reduced as a result of deeper signal penetration and lower sensitivity to surface roughness. The original scattering models at P-band frequencies displayed large variability, with substantial underestimation by both the AIEM and Oh models at 860 MHz and considerable scatter across all models at 440 MHz. These results highlight the inherent difficulty of accurately modeling subsurface scattering at lower frequencies

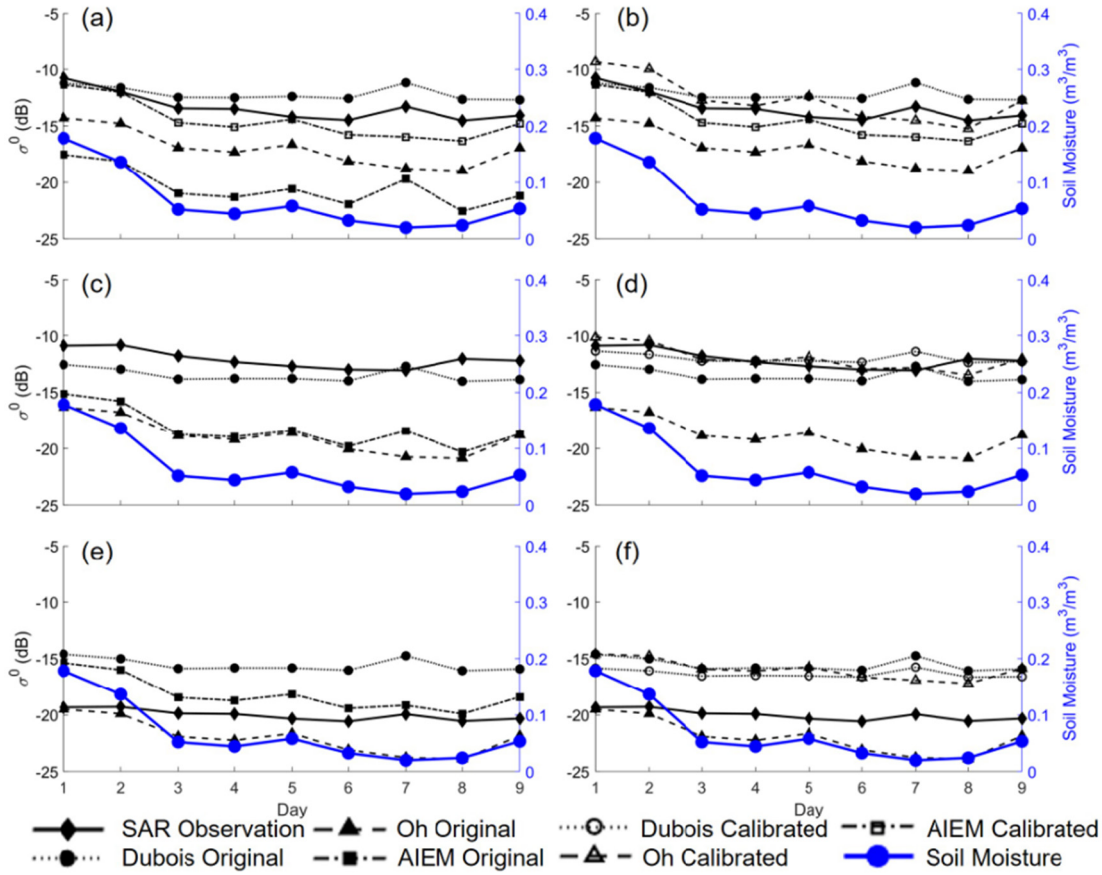


Fig. 7. Time series of the observed and simulated daily average backscatter coefficient $\sigma^0$ for HH polarization and near-surface soil moisture over nine days in the APPLEx-1 YB area. Corresponding to the three frequencies as follows. (a) PLIS at 1.26 GHz under scenario 1 (S1). (b) PLIS at 1.26 GHz under scenario 2 (S2). (c) PPIS at 860 MHz under S1. (d) PPIS at 860 MHz under S2. (e) PPIS at 440 MHz under S1. (f) PPIS at 440 MHz under S2. Each panel includes SAR observations, original model outputs, and scenario-specific simulations. Soil moisture is shown on the secondary $y$-axis in (e) and (f).

using surface scattering models. Calibration improved the agreement between modeled and observed $\sigma^0$, with scenario 1 scattering models typically showing lower biases. Nevertheless, the calibrated scattering models, especially for scenario 2, still exhibited considerable differences at P-band, underscoring the limitation of using surface-only scattering models at these lower frequencies.

## V. Discussion

This study made a comprehensive evaluation and calibration of commonly used surface scattering models, with a focus on P-band at 440 and 860 MHz. The performance of the original semi-empirical scattering models varied notably across frequency bands. At C- and S-bands, scattering model accuracy was constrained by the narrow range of soil moisture and the limited size of the available datasets. Despite these limitations, both the Dubois and Oh models showed potential for simulating SAR observations, particularly after calibration.

At L-band, the original Dubois and Oh models exhibited reliable performance, achieving high correlation and low RMSE values for a range of soil and observation conditions. However, evaluation of the original AIEM showed relatively large RMSE values, consistent with results from previous studies. For instance, Choker et al. [26] reported that when using L-band spaceborne SAR, the Dubois model achieved the lowest RMSE (2.5 dB in VV polarization), followed by the Oh model, which exhibited a slight overestimation of 1–2 dB. In contrast, the AIEM model consistently underestimated $\sigma^0$, resulting in the highest RMSE (approximately 5.9 dB in VV). Similarly, Panciera et al. [25], using the same L-band airborne SAR instrumentation, found that the Oh model best matched observations, followed by the Dubois and IEM models, with the largest mean error of 7.1 dB observed for IEM VV polarization.

These comparisons confirm that the semi-empirical Dubois and Oh scattering models are generally reliable at L-band, but can still exhibit overestimation or underestimation depending on site-specific conditions. In contrast, the physical AIEM and IEM models often underperform due to their sensitivity to surface roughness parameters, particularly the correlation length, which is notoriously difficult to measure accurately in field conditions. In order to address such a matter, multiscale methods have been introduced to better represent surface roughness. However, since the study area primarily consists of natural grassland, large-scale roughness features such as row structures commonly found in agricultural fields are absent. Therefore, the application of multiscale models was considered unnecessary in this context.

Calibration led to clear improvements in scattering model performance across most frequencies. At L-, C-, and S-bands, the calibrated scattering models showed reduced RMSE and bias. The AIEM model, in particular, benefited from the introduction of an optimized roughness parameter ($L_{opt}$), replacing the traditional correlation length. This adjustment led to substantial reductions in RMSE and bias, especially at S-band (RMSE 2.1 dB) and C-band (bias reduced by 16 dB and RMSE 5.9 dB). Using averaged $L_{opt}$ values derived from L- and C-band at S-band also yielded favorable results. At L-band, RMSE improved to approximately 2.3 dB, highlighting the effectiveness of semi-empirical calibration even for a physical scattering model like the AIEM.

At P-band frequencies (860 and 440 MHz), scattering model performance varied substantially across calibration scenarios, aligning with current understanding. Specifically, under dry surface conditions, the deeper penetration at P-band frequencies can lead to dominance by subsurface scattering (Fig. 4). Conversely, when the surface is wet, penetration is reduced, allowing near-surface soil moisture to dominate over subsurface scattering [54].

Under scenario 1, the Dubois and Oh models performed comparably well after calibration, achieving low RMSE at both P-band frequencies. These results suggest that under stable spatial and temporal conditions, semi-empirical scattering models can be extended to lower frequencies, despite their inherent limitations in capturing deeper signal penetration and subsurface scattering. However, despite the reduced RMSE, the correlation coefficients at 860 MHz remained below 0.2 for both scattering models. This indicates that while calibration may improve scattering model accuracy in terms of magnitude, it does not necessarily enhance the ability to capture the temporal dynamics of $\sigma^0$, especially when subsurface contributions become substantial. These findings highlight the flexibility of the Dubois and Oh empirical models in simulating P-band $\sigma^0$ under controlled conditions, but also their fundamental limitations in representing the physics of P-band scattering.

Under scenario 2, the scattering model performance deteriorated. RMSE increased by more than 0.5 dB, and biases at 440 MHz rose to approximately 4 dB. These results underscore the challenge of using semi-empirical scattering models under broader temporal and spatial variability. The decline in performance suggests that these scattering models may lack the robustness needed to generalize across diverse environmental conditions at low frequencies.

The AIEM model failed to perform adequately at both of the P-band frequencies, even after an attempted calibration of the $L_{opt}$ parameter. This scattering model persistently underestimated $\sigma^0$, and no empirically derived $L_{opt(P)}$ value was able to reconcile the simulated and observed backscatter at P-band. This trend became more pronounced at 440 MHz, supporting the notion that subsurface scattering, which increases with decreasing frequency, may not be effectively represented by surface-only scattering models like the AIEM. A more suitable approach would involve multilayer physical models, such as a multilayered small perturbation model [55], though such methods fall beyond the scope of this study.

## VI. Conclusion

This study evaluated the performance of three commonly used radar-surface scattering models, including the semi-empirical Dubois and Oh models and the physical AIEM model, across five radar frequencies (C-, S-, L-, and two different P-bands) using a combination of airborne and spaceborne SAR datasets. The scattering models were assessed under two scenarios to investigate their performance across different spatial and temporal conditions, providing key insights into their capabilities and limitations.

At P-band frequencies, weak correlations were found between SAR observations and scattering model outputs at 860 MHz, as well as between SAR observations and soil moisture measurements at 440 MHz. This finding suggests substantial subsurface scattering effects at these frequencies due to their longer wavelengths. Both the original Dubois and original Oh models showed limited accuracy at P-band, with biases reaching around 6 dB and RMSE values up to 7.5 dB. After calibration using datasets collected under stable conditions, these scattering models, especially the Dubois model, demonstrated improved adaptability, resulting in substantially reduced bias and RMSE values, being mostly below 2 dB. However, performance declined when the scattering models were applied to datasets representing more variable conditions, with the RMSE increasing to about 2.5 dB for the Dubois model and approximately 4 dB for the Oh model. This variability highlights challenges faced by semi-empirical models in accurately characterizing scattering processes at P-band frequencies.

The AIEM model is also ineffective at P-band, as its physical assumptions focused solely on surface scattering, neglecting the substantial subsurface contributions observed at these longer wavelengths, especially in dry conditions where subsurface scattering could dominate. These findings emphasize the need for multilayered physical scattering models that incorporate subsurface effects to accurately represent wave interactions at P-band frequencies. Future research should therefore focus on implementing such models to enhance the accuracy and applicability of soil moisture retrieval across diverse environmental conditions.

## Acknowledgment

The authors extend gratitude to numerous volunteers for their valuable contributions in data collection during the PRISM21 and APPLEx-1 experiments used in this study. The portion of work described in this publication carried out at the Jet Propulsion Laboratory, California Institute of Technology, is under a contract with the National Aeronautics and Space Administration.

## References

[1] H. Vereecken, J. A. Huisman, H. Bogena, J. Vanderborght, J. A. Vrugt, and J. W. Hopmans, "On the value of soil moisture measurements in vadose zone hydrology: A review," *Water Resour. Res.*, vol. 44, no. 4, Apr. 2008, Art. no. W00D06, doi: 10.1029/2008wr006829.

[2] J. Peng et al., "A roadmap for high-resolution satellite soil moisture applications—Confronting product characteristics with user requirements," *Remote Sens. Environ.*, vol. 252, Jan. 2021, Art. no. 112162, doi: 10.1016/j.rse.2020.112162.

[3] E. T. Engman and N. Chauhan, "Status of microwave soil moisture measurements with remote sensing," *Remote Sens. Environ.*, vol. 51, no. 1, pp. 189–198, Jan. 1995, doi: 10.1016/0034-4257(94)00074-w.

[4] V. L. Mironov, M. C. Dobson, V. H. Kaupp, S. A. Komarov, and V. N. Kleshchenko, "Generalized refractive mixing dielectric model for moist soils," *IEEE Trans. Geosci. Remote Sens.*, vol. 42, no. 4, pp. 773–785, Apr. 2004, doi: 10.1109/TGRS.2003.823288.

[5] V. L. Mironov, P. P. Bobrov, and S. V. Fomin, "Multirelaxation generalized refractive mixing dielectric model of moist soils," *IEEE Geosci. Remote Sens. Lett.*, vol. 10, no. 3, pp. 603–606, May 2013, doi: 10.1109/LGRS.2012.2215574.

[6] L. Zhu, S. Yuan, Y. Liu, C. Chen, and J. P. Walker, "Time series soil moisture retrieval from SAR data: Multi-temporal constraints and a global validation," *Remote Sens. Environ.*, vol. 287, Mar. 2023, Art. no. 113466, doi: 10.1016/j.rse.2023.113466.

[7] L. Zhu, J. Dai, Y. Liu, S. Yuan, T. Qin, and J. P. Walker, "A cross-resolution transfer learning approach for soil moisture retrieval from Sentinel-1 using limited training samples," *Remote Sens. Environ.*, vol. 301, Feb. 2024, Art. no. 113944, doi: 10.1016/j.rse.2023.113944.

[8] O. Merlin, A. Chehbouni, Y. H. Kerr, and D. C. Goodrich, "A downscaling method for distributing surface soil moisture within a microwave pixel: Application to the monsoon '90 data," *Remote Sens. Environ.*, vol. 101, no. 3, pp. 379–389, Apr. 2006, doi: 10.1016/j.rse.2006.01.004.

[9] J. Dari, L. Brocca, P. Quintana-Seguí, M. J. Escorihuela, V. Stefan, and R. Morbidelli, "Exploiting high-resolution remote sensing soil moisture to estimate irrigation water amounts over a Mediterranean region," *Remote Sens.*, vol. 12, no. 16, p. 2593, Aug. 2020, doi: 10.3390/rs12162593.

[10] L. Zhu, R. Si, X. Shen, and J. P. Walker, "An advanced change detection method for time-series soil moisture retrieval from Sentinel-1," *Remote Sens. Environ.*, vol. 279, Sep. 2022, Art. no. 113137, doi: 10.1016/j.rse.2022.113137.

[11] R. Magagi, S. Jammali, K. Goïta, H. Wang, and A. Colliander, "Potential of L{-} and C-bands polarimetric SAR data for monitoring soil moisture over forested sites," *Remote Sens.*, vol. 14, no. 21, p. 5317, Oct. 2022, doi: 10.3390/rs14215317.

[12] T. Le Toan et al., "The BIOMASS mission: Mapping global forest biomass to better understand the terrestrial carbon cycle," *Remote Sens. Environ.*, vol. 115, no. 11, pp. 2850–2860, Nov. 2011, doi: 10.1016/j.rse.2011.03.020.

[13] P. A. Rosen et al., "The NASA-ISRO SAR mission—An international space partnership for science and societal benefit," in *Proc. IEEE Radar Conf. (RadarCon)*, May 2015, pp. 1610–1613, doi: 10.1109/RADAR.2015.7131255.

[14] A. Held, Z.-S. Zhou, C. Ticehurst, A. Rosenqvist, A. Parker, and L. Brindle, "Advancing Australia's imaging radar capability under the Novasar-1 partnership," in *Proc. IEEE Int. Geosci. Remote Sens. Symp.*, Jul. 2019, pp. 8370–8373, doi: 10.1109/IGARSS.2019.8898623.

[15] A. Tabatabaeenejad, M. Burgin, X. Duan, and M. Moghaddam, "P-band radar retrieval of subsurface soil moisture profile as a second-order polynomial: First AirMOSS results," *IEEE Trans. Geosci. Remote Sens.*, vol. 53, no. 2, pp. 645–658, Feb. 2015, doi: 10.1109/TGRS.2014.2326839.

[16] P. C. Dubois, J. van Zyl, and T. Engman, "Measuring soil moisture with imaging radars," *IEEE Trans. Geosci. Remote Sens.*, vol. 33, no. 4, pp. 915–926, Jul. 1995, doi: 10.1109/36.406677.

[17] P. C. Dubois, J. van Zyl, and T. Engman, "Corrections to 'Measuring soil moisture with imaging radars," *IEEE Trans. Geosci. Remote Sens.*, vol. 33, no. 6, p. 1340, Nov. 1995, doi: 10.1109/TGRS.1995.477194.

[18] Y. Oh, K. Sarabandi, and F. T. Ulaby, "An empirical model and an inversion technique for radar scattering from bare soil surfaces," *IEEE Trans. Geosci. Remote Sens.*, vol. 30, no. 2, pp. 370–381, Mar. 1992, doi: 10.1109/36.134086.

[19] Y. Oh, K. Sarabandi, and F. T. Ulaby, "An inversion algorithm for retrieving soil moisture and surface roughness from polarimetric radar observation," in *Proc. IEEE Int. Geosci. Remote Sens. Symp.*, Mar. 1994, pp. 1582–1584, doi: 10.1109/IGARSS.1994.399504.

[20] Y. Oh, K. Sarabandi, and F. T. Ulaby, "Semi-empirical model of the ensemble-averaged differential Mueller matrix for microwave backscattering from bare soil surfaces," *IEEE Trans. Geosci. Remote Sens.*, vol. 40, no. 6, pp. 1348–1355, Jun. 2002, doi: 10.1109/TGRS.2002.800232.

[21] Y. Oh, "Quantitative retrieval of soil moisture content and surface roughness from multipolarized radar observations of bare soil surfaces," *IEEE Trans. Geosci. Remote Sens.*, vol. 42, no. 3, pp. 596–601, Mar. 2004, doi: 10.1109/TGRS.2003.821065.

[22] A. K. Fung, Z. Li, and K. S. Chen, "Backscattering from a randomly rough dielectric surface," *IEEE Trans. Geosci. Remote Sens.*, vol. 30, no. 2, pp. 356–369, Mar. 1992, doi: 10.1109/36.134085.

[23] T.-D. Wu and K.-S. Chen, "A reappraisal of the validity of the IEM model for backscattering from rough surfaces," *IEEE Trans. Geosci. Remote Sens.*, vol. 42, no. 4, pp. 743–753, Apr. 2004, doi: 10.1109/TGRS.2003.815405.

[24] N. Baghdadi and M. Zribi, "Evaluation of radar backscatter models IEM, Oh and Dubois using experimental observations," *Int. J. Remote Sens.*, vol. 27, no. 18, pp. 3831–3852, Sep. 2006, doi: 10.1080/01431160600658123.

[25] R. Panciera, M. A. Tanase, K. Lowell, and J. P. Walker, "Evaluation of IEM, Dubois, and Oh radar backscatter models using airborne L-band SAR," *IEEE Trans. Geosci. Remote Sens.*, vol. 52, no. 8, pp. 4966–4979, Aug. 2014, doi: 10.1109/TGRS.2013.2286203.

[26] M. Choker et al., "Evaluation of the Oh, Dubois and IEM backscatter models using a large dataset of SAR data and experimental soil measurements," *Water*, vol. 9, no. 1, p. 38, Jan. 2017, doi: 10.3390/w9010038.

[27] H. Lievens, H. Vernieuwe, J. Álvarez-Mozos, B. De Baets, and N. E. C. Verhoest, "Error in radar-derived soil moisture due to roughness parameterization: An analysis based on synthetical surface profiles," *Sensors*, vol. 9, no. 2, pp. 1067–1093, Feb. 2009, doi: 10.3390/s90201067.

[28] Y. Oh and Y. Chul Kay, "Condition for precise measurement of soil surface roughness," *IEEE Trans. Geosci. Remote Sens.*, vol. 36, no. 2, pp. 691–695, Mar. 1998, doi: 10.1109/36.662751.

[29] G. Di Martino, A. Di Simone, and A. Iodice, "A novel analytical formulation of the correlation of GNSS-R signals scattered by a natural fractal surface," *IEEE Geosci. Remote Sens. Lett.*, vol. 21, pp. 1–5, 2024, doi: 10.1109/LGRS.2024.3365357.

[30] S. T. Wu and A. K. Fung, "A noncoherent model for microwave emissions and backscattering from the sea surface," *J. Geophys. Res.*, vol. 77, no. 30, pp. 5917–5929, Oct. 1972, doi: 10.1029/jc077i030p05917.

[31] S. H. Yueh, "Modeling of wind direction signals in polarimetric sea surface brightness temperatures," *IEEE Trans. Geosci. Remote Sens.*, vol. 35, no. 6, pp. 1400–1418, Nov. 1997, doi: 10.1109/36.649793.

[32] N. Baghdadi, C. King, A. Chanzy, and J. P. Wigneron, "An empirical calibration of the integral equation model based on SAR data, soil moisture and surface roughness measurement over bare soils," *Int. J. Remote Sens.*, vol. 23, no. 20, pp. 4325–4340, Jan. 2002, doi: 10.1080/01431160110107671.

[33] N. Baghdadi, N. Holah, and M. Zribi, "Calibration of the integral equation model for SAR data in C-band and HH and VV polarizations," *Int. J. Remote Sens.*, vol. 27, no. 4, pp. 805–816, Feb. 2006, doi: 10.1080/01431160500212278.

[34] N. Baghdadi, I. Gherboudj, M. Zribi, M. Sahebi, C. King, and F. Bonn, "Semi-empirical calibration of the IEM backscattering model using radar images and moisture and roughness field measurements," *Int. J. Remote Sens.*, vol. 25, no. 18, pp. 3593–3623, Sep. 2004, doi: 10.1080/01431160310001654392.

[35] N. Baghdadi et al., "Semi-empirical calibration of the integral equation model for co-polarized L-band backscattering," *Remote Sens.*, vol. 7, no. 10, pp. 13626–13640, Oct. 2015, doi: 10.3390/rs71013626.

[36] X. Bai, B. He, and X. Li, "Optimum surface roughness to parameterize advanced integral equation model for soil moisture retrieval in Prairie area using Radarsat-2 data," *IEEE Trans. Geosci. Remote Sens.*, vol. 54, no. 4, pp. 2437–2449, Apr. 2016, doi: 10.1109/TGRS.2015.2501372.

[37] A. Balenzano et al., "Sentinel-1 soil moisture at 1 km resolution: A validation study," *Remote Sens. Environ.*, vol. 263, Sep. 2021, Art. no. 112554, doi: 10.1016/j.rse.2021.112554.

[38] L. Zhu et al., "The polarimetric L-band imaging synthetic aperture radar (PLIS): Description, calibration, and cross-validation," *IEEE J. Sel. Topics Appl. Earth Observ. Remote Sens.*, vol. 11, no. 11, pp. 4513–4525, Nov. 2018.

[39] A. Balenzano, F. Mattia, G. Satalino, V. Pauwels, and P. Snoeij, "SMOSAR algorithm for soil moisture retrieval using Sentinel-1 data," in *Proc. IEEE Int. Geosci. Remote Sens. Symp.*, Mar. 2012, pp. 1200–1203, doi: 10.1109/IGARSS.2012.6351332.

[40] L. Karthikeyan, M. Pan, N. Wanders, D. N. Kumar, and E. F. Wood, "Four decades of microwave satellite soil moisture observations: Part 1. A review of retrieval algorithms," *Adv. Water Resour.*, vol. 109, pp. 106–120, Nov. 2017, doi: 10.1016/j.advwatres.2017.09.006.

[41] M. Sadeghi, A. Tabatabaeenejad, M. Tuller, M. Moghaddam, and S. Jones, "Advancing NASA's AirMOSS P-Band radar root zone soil moisture retrieval algorithm via incorporation of Richards' equation," *Remote Sens.*, vol. 9, no. 1, p. 17, Dec. 2016, doi: 10.3390/rs9010017.

[42] A. Tabatabaeenejad et al., "Assessment and validation of AirMOSS P-band root-zone soil moisture products," *IEEE Trans. Geosci. Remote Sens.*, vol. 58, no. 9, pp. 6181–6196, Sep. 2020, doi: 10.1109/TGRS.2020.2974976.
[43] R. Torres et al., "GMES Sentinel-1 mission," *Remote Sens. Environ.*, vol. 120, pp. 9–24, May 2012, doi: 10.1016/j.rse.2011.05.028.
[44] O. Merlin, J. Walker, R. Panciera, R. Young, J. Kalma, and E. Kim, "Soil moisture measurement in heterogeneous terrain," in *Proc. Int. Congr. Model. Simul.*, Dec. 2007, pp. 2604–2610.
[45] Q. Wang, T. Jin, J. Li, X. Chang, Y. Li, and Y. Zhu, "Modeling and assessment of vegetation water content on soil moisture retrieval via the synergistic use of Sentinel-1 and Sentinel-2," *Earth Space Sci.*, vol. 9, no. 5, May 2022, Art. no. EA002063, doi: 10.1029/2021ea002063.
[46] N. Baghdadi, P. Paillou, G. Grandjean, P. Dubois, and M. Davidson, "Relationship between profile length and roughness variables for natural surfaces," *Int. J. Remote Sens.*, vol. 21, no. 17, pp. 3375–3381, Jan. 2000, doi: 10.1080/014311600750019994.
[47] E. Schanda, *Physical Fundamentals of Remote Sensing*. Cham, Switzerland: Springer, 1986.
[48] N. E. C. Verhoest, H. Lievens, W. Wagner, J. Álvarez-Mozos, M. S. Moran, and F. Mattia, "On the soil roughness parameterization problem in soil moisture retrieval of bare surfaces from synthetic aperture radar," *Sensors*, vol. 8, no. 7, pp. 4213–4248, Jul. 2008, doi: 10.3390/s8074213.
[49] M. Dobson, F. Ulaby, M. Hallikainen, and M. El-rayes, "Microwave dielectric behavior of wet soil-part II: Dielectric mixing models," *IEEE Trans. Geosci. Remote Sens.*, vols. GE-23, no. 1, pp. 35–46, Jan. 1985, doi: 10.1109/TGRS.1985.289498.
[50] X. Zhang, B. Chen, H. Fan, J. Huang, and H. Zhao, "The potential use of multi-band SAR data for soil moisture retrieval over bare agricultural areas: Hebei, China," *Remote Sens.*, vol. 8, no. 1, p. 7, Dec. 2015, doi: 10.3390/rs8010007.
[51] K. S. Chen, T.-D. Wu, L. Tsang, Q. Li, J. Shi, and A. K. Fung, "Emission of rough surfaces calculated by the integral equation method with comparison to three-dimensional moment method simulations," *IEEE Trans. Geosci. Remote Sens.*, vol. 41, no. 1, pp. 90–101, Jan. 2003, doi: 10.1109/TGRS.2002.807587.
[52] N. Baghdadi, E. Saba, M. Aubert, M. Zribi, and F. Baup, "Evaluation of radar backscattering models IEM, Oh, and Dubois for SAR data in X-band over bare soils," *IEEE Geosci. Remote Sens. Lett.*, vol. 8, no. 6, pp. 1160–1164, Nov. 2011, doi: 10.1109/LGRS.2011.2158982.
[53] N. Baghdadi, J. Abou Chaaya, and M. Zribi, "Semiempirical calibration of the integral equation model for SAR data in C-band and cross polarization using radar images and field measurements," *IEEE Geosci. Remote Sens. Lett.*, vol. 8, no. 1, pp. 14–18, Jan. 2011, doi: 10.1109/LGRS.2010.2050054.
[54] F. Brakhasi et al., "Soil moisture profile estimation under bare and vegetated soils using combined L-band and P-band radiometer observations: An incoherent modeling approach," *Remote Sens. Environ.*, vol. 307, Jun. 2024, Art. no. 114148, doi: 10.1016/j.rse.2024.114148.
[55] A. Tabatabaeenejad and M. Moghaddam, "Bistatic scattering from three-dimensional layered rough surfaces," *IEEE Trans. Geosci. Remote Sens.*, vol. 44, no. 8, pp. 2102–2114, Aug. 2006, doi: 10.1109/TGRS.2006.872140.
[56] M. Mancini, R. Hoeben, and P. A. Troch, "Multifrequency radar observations of bare surface soil moisture content: A laboratory experiment," *Water Resour. Res.*, vol. 35, no. 6, pp. 1827–1838, Jun. 1999.

**Ziwei Xiong** received the B.E. degree (Hons.) in civil engineering from Monash University, Melbourne, VIC, Australia, in 2022, where he is currently pursuing the Ph.D. degree in civil engineering.

In 2023, he was a Visiting Ph.D. Student at the University of Southern California, Los Angeles, CA, USA. His research interests include active microwave remote sensing and root-zone soil moisture retrieval.

**Jeffrey P. Walker** (Fellow, IEEE) received the B.E. (civil) and B.Surveying degrees and (Hons.) and the Ph.D. degree in water resources engineering from The University of Newcastle, Callaghan, NSW, Australia, in 1996 and 2000, respectively.

His Ph.D. thesis was among the early pioneering research on estimation of root-zone soil moisture from assimilation of remotely sensed surface soil moisture observations. He then joined the NASA Goddard Space Flight Centre, Greenbelt, MD, USA, to implement his soil moisture work globally. In 2001, he was a Lecturer at the Department of Civil and Environmental Engineering, University of Melbourne, Parkville, VIC, Australia, where he continued his soil moisture work, including the development of the only Australian airborne capability for simulating new satellite missions for soil moisture. In 2010, he was appointed as a Professor at the Department of Civil Engineering and Environmental Engineering, Monash University, Melbourne, VIC, Australia, where he has continued this research. He is contributing to soil moisture satellite missions at NASA, ESA, and JAXA, as a Science Team Member for the Soil Moisture Active Passive (SMAP) Mission Cal/val Team Member for the Soil Moisture and Ocean Salinity (SMOS) and Global Change Observation Mission—Water (GCOM-W).

Dr. Walker is a Laureate Fellow of Australian Research Council. During the bachelor's degree, he received the University Medal from The University of Newcastle.

**Liujun Zhu** (Member, IEEE) received the B.S. degree in geography from Zhejiang Normal University, Jinhua, China, in 2012, the M.Sc. degree in geography information science from Nanjing University, Nanjing, China, in 2015, and the Ph.D. degree in civil engineering from Monash University, Melbourne, VIC, Australia, in 2019, with a thesis on multi-SAR soil moisture retrieval.

From 2017 to 2018, he was a Visiting Scholar with the University of Michigan–Ann Arbor, Ann Arbor, MI, USA. From 2019 to 2020, he continued his research on radar soil moisture as a Research Fellow with Monash University, where he has been held an adjunct position since 2020. He is currently an Associate Professor at the Yangtze Institute for Conservation and Development, Hohai University, Nanjing. His research interests include microwave remote sensing of soil moisture and machine learning and its applications in soil moisture studies.

**Brian Ng** (Member, IEEE) received the B.Ma&CompSc degree, the B.E. degree in electrical and electronic engineering, and the Ph.D. degree in electronic engineering from the University of Adelaide, Adelaide, SA, Australia, in 1996, 1997, and 2003, respectively.

He is currently an Associate Professor with the School of Electrical and Mechanical Engineering, Adelaide University. His research interests include radar imaging, radar signal processing, and time-frequency techniques.

Dr. Ng was awarded the University of Adelaide Medal for the top graduate in electrical and electronic engineering. He is an Associate Editor of IEEE TRANSACTIONS ON RADAR SYSTEMS and IEEE SIGNAL PROCESSING LETTERS. He is a Regular Reviewer of IEEE TRANSACTIONS ON AEROSPACE AND ELECTRONIC SYSTEMS, *IET Radar, Sonar and Navigation*, and international radar conferences.

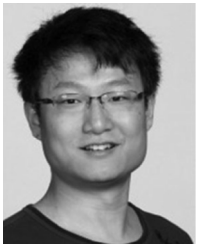

**Nan Ye** received the B.E. degree in hydraulic and hydropower engineering from Tsinghua University, Beijing, China, in 2006, and the Ph.D. degree in civil engineering from Monash University, Melbourne, VIC, Australia, in 2014.

Then, he coordinated several airborne field experiments for the in-orbit calibration/validation of the Soil Moisture Active Passive Mission and the development of P-band soil moisture remote sensing techniques in the Murrumbidgee River catchment, Southeast of Australia. Since 2025, he has been a Lecturer and a Research Fellow at Monash Suzhou Science and Technology Research Institute, Suzhou, China, focusing on microwave remote sensing of soil moisture.

**Xiaoling Wu** (Senior Member, IEEE) received the B.E. degree in biomedical engineering from Zhejiang University, Hangzhou, China, in 2009, and the Ph.D. degree in civil engineering from Monash University, Clayton, Melbourne, VIC, Australia, in 2015.

Her undergraduate thesis was the development of biosensor using nanomaterial. She was a Visiting Scholar with the Department of Computer Science, University of Copenhagen, Copenhagen, Denmark, from 2009 to 2010. The topic of her Ph.D. Research was downscaling of soil moisture (SM) using airborne radar and radiometer observations in order to provide an accurate and high-resolution (better than 10 km) SM product with potential benefit in the areas of weather forecasting, flood, drought prediction, and agricultural activities. She is a Research Fellow with Monash University and continues high-resolution SM work. Her research interests include microwave remote sensing of SM, SM downscaling, and proximal SM sensing for real-time agricultural applications.

**Lixiaozhou Zhou** (Member, IEEE) received the M.E. degree (Hons.) from the University of Melbourne, Parkville, VIC, Australia, in 2018, and the Ph.D. degree in environmental engineering from Monash University, Clayton, Melbourne, VIC, Australia, in 2025.

She was a Visiting Scholar with the Ming Hsieh Department of Electrical and Computer Engineering, University of Southern California, Los Angeles, CA, USA. Since 2025, she has been a Research Fellow with Monash University. Her research interests include active and passive microwave remote sensing and their applications in soil moisture retrieval and soil moisture downscaling.

**Luisa F. White-Murillo** (Member, IEEE) received the bachelor's degree in surveying engineering from the Universidad Distrital Francisco Jose de Caldas, Bogota, Colombia, in 2015, and the Master of Advanced Civil Engineering (Water) and Ph.D. degrees in civil engineering from Monash University, Melbourne, VIC, Australia, in 2020 and 2026, respectively.

Her research has focused on the estimation of high-resolution root-zone soil moisture using L- and P-band passive and active microwave remote sensing. Her research interests include microwave and hyperspectral remote sensing for monitoring water resources and vegetation.

**James Hills** received the B.Rur.Sci. (Hons.) and Ph.D. degrees from the University of New England, Armidale, NSW, Australia, in 1996 and 2000, respectively.

He is currently an Associate Professor and the Livestock Production Centre Leader at Tasmanian Institute of Agriculture, University of Tasmania, Hobart, TAS, Australia. His research focuses on the sustainable use of inputs for pasture-based dairy systems, specifically regarding nitrogen and water management. He has a particular interest in farming system variability and the integration of technology for measuring and managing such variability to enhance production efficiency and sustainability.

**Mahta Moghaddam** (Fellow, IEEE), photograph and biography not available at the time of publication.

**Simon Yueh** (Fellow, IEEE) received the Ph.D. degree in electrical engineering from Massachusetts Institute of Technology, Cambridge, MA, USA, in January 1991.

He was a Post-Doctoral Research Associate at Massachusetts Institute of Technology from February to August 1991. In September 1991, he joined the Radar Science and Engineering Section, Jet Propulsion Laboratory (JPL), Pasadena, CA, USA. He was a Supervisor with the Radar System Engineering and Algorithm Development Group from 2002 to 2007, the Deputy Manager of the Climate, Oceans, and Solid Earth Section from July 2007 to March 2009, and the Section Manager from April 2009 to January 2013. He was the Project Scientist of the National Aeronautics and Space Administration (NASA) Aquarius Mission from January 2012 to September 2013 and the Deputy Project Scientist of NASA Soil Moisture Active Passive Mission from January 2013 to September 2013. He has been an SMAP Project Scientist since October 2013. He has been the principal/co-investigator of numerous NASA and DOD research projects on remote sensing of ocean salinity, ocean wind, terrestrial snow, and soil moisture. He has authored four book chapters and published more than 300 publications and presentations.

Dr. Yueh is a member of URSI Commission-F. He received the 2021 IEEE J-STARS Prize Paper Award, the 2014 IEEE GRSS Transaction Prize Paper Award, the 2010 IEEE GRSS Transaction Prize Paper Award, the 2002 IEEE GRSS Transaction Prize Paper Award, the 2000 Best Paper Award in the IEEE International Geoscience and Remote Symposium 2000, and the 1995 IEEE GRSS Transaction Prize Paper Award for a paper on polarimetric radiometry. He received the JPL Lew Allen Award in 1998, the Ed Stone Award in 2003 and 2023, and the IEEE GRSS Service Award in 2023. He was an Associate Editor of *Radio Science* from 2002 to 2006 and the Editor-in-Chief of IEEE TRANSACTIONS ON GEOSCIENCE AND REMOTE SENSING from 2018 to 2022.